Role of Stress-Driven Interfacial Instability in the Failure of Confined Electric Interconnects

Nan Wang and Nikolas Provatas

Department of Physics and Center for the Physics of Materials, McGill University, Montreal, Québec H3A 2T8, Canada

(Received 24 October 2016; revised manuscript received 31 January 2017; published 28 February 2017)

We examine the possible role of stress-driven surface instability in the failure of electric interconnects found in large-scale integrated circuits. While electromigration is commonly known as the main reason behind interconnect failure, the complex interplay of electromigration-induced mass transport and stress-induced transport has also been studied extensively since the discovery of the Blech effect due to its importance in integrated-circuit design. However, the role of the dielectric medium confining the interconnect has not been properly included in previous analysis of this phenomenon. Here, we examine the classic ATG instability in the presence of dielectric confinement. We propose that thermal stress and surface transport, typically active in all metal interconnects, may trigger a surface instability at the metal-dielectric interface. In particular, we show that there exists a critical thermal stress level below which the stress-driven surface instability cannot be responsible for the failure of interconnects of any length. However, for an interconnect confined by soft low-k dielectric materials, thermal stresses can still be large enough that such stress-driven instability may break the metal conductor even if its length is below the Blech limit.

DOI: 10.1103/PhysRevApplied.7.024032

I. INTRODUCTION

Electromigration (EM) is a major reliability concern in electric circuit design. Because of the momentum transfer of scattered conducting electrons, lattice atoms in metal conductor are subject to a significant electromigration force at large electric-current density. Within an electric interconnect, the electromigration force can induce local void nucleation and extrusion formation, and eventually lead to catastrophic circuit failure. Understanding EM and other associated circuit-failure phenomena is becoming increasingly important as integrated-circuit technologies move towards ever-higher density.

Phenomenologically, the effect of electromigration is described by a force $f_{\mathrm{em}} = Z^* eE$ acting on atoms of a metallic conductor, where e is the electron charge, E is the local electric field, and Z^* is a number known as the effective EM charge [1–3]. It is well known that under the same current density, interconnects are more likely to fail as their length increases. This length-dependent failure phenomenon is known as the Blech effect, which results from the competition of EM-induced atom transport from cathode to anode and stress-induced transport in the opposite direction. The Blech effect can be described using a one-dimensional transport equation of interconnect atoms

$$\frac{\partial C}{\partial t} = \frac{\partial}{\partial x}\left[D\left(\frac{\partial C}{\partial x} - C\frac{Z^* e j\rho}{kT} + C\frac{\Omega}{kT}\frac{\partial \sigma}{\partial x}\right)\right], \qquad (1)$$

where C is the concentration of atoms per unit volume, D is the diffusion coefficient, kT is thermal energy, σ is the hydrostatic stress, j is the electric-current density, ρ is the resistivity, and Ω is the atomic volume. Equation (1) describes three competing effects, solute diffusion, the EM-induced force f_{em}, and an additional force f_{con} on atoms due to the confinement stress of the surrounding materials. The latter is typically formulated using the chemical potential of atoms under stress $\mu = \Omega\sigma$. The force induced by the confinement is then given by the gradient of this chemical potential $f_{\mathrm{con}} = -\nabla\mu = -d\Omega\sigma/dx$. It follows that the two forces introduced by EM and confinement stress may cancel out each other if

$$jl_B = \frac{\Omega\sigma_m}{Z^* e\rho}, \qquad (2)$$

where σ_m is the maximum stress the interconnect can support between the cathode and anode ends, and the length l_B is known as the Blech length, or, more generally, jl_B is called the Blech product [4,5]. The Blech length given in Eq. (2) represents the length limit of an interconnect beyond which the confinement stress from surrounding dielectrics is not enough to stop the EM-induced atom transport. As a result, continuous pileup of atoms at the anode side and depletion at the cathode side will cause extrusion and void nucleation, and eventually lead to interconnect failure. Equation (2) is used as a primary guideline in integrated-circuit (IC) design in order to minimize EM-induced circuit failure. Commercial IC's typically use elastically soft low-k materials, and experimental measurements have found that interconnects

surrounded by low-k dielectric materials are the most prone to EM-induced failure [6,7]. Three major failure modes, extrusion, voiding, and delamination, have been proposed as the limiting factor of the maximum stress σ_m in interconnects [8–10].

Another form of stress that is present in IC's during manufacturing is that of thermal stress. The interplay of thermal stress migration (TSM) and EM has been shown to have significant impact on the mean-time-to-failure of electric circuits in many experimental and theoretical works [11–18]. Since the TSM effect can be active without electric current when circuits are stored at elevated temperatures [19], many theories use TSM to describe void nucleation when addressing the stress-voiding phenomenon in interconnects [8,20]. On the other hand, it is well known that stress can also drive the motion of interfaces in the solid state, promote second-phase nucleation, and cause surface instability [21]. Thermally induced surface instability, caused by the rearrangement of surface atoms following the gradient of local elastic energy density, may be particularly relevant to interconnect failure as it will contribute to the stress-driven transport mechanism in the Blech effect.

The aforementioned stress-driven surface instability is known as Araso-Tiller-Grinfeld (ATG) instability [22,23] and is mostly studied in the context of thin film materials. In the classic 2D setup where the solid material is under mode I external stress σ_0 along the x direction and has a free surface with surface normal along y, stability analysis shows that there exists a critical length l_c (along the x direction) of the solid material beyond which a small amplitude long wavelength perturbation to the surface shape will be amplified and eventually break the material. The salient physics of ATG involves the competition of two atom fluxes along the surface. One is generated by the difference of local stress near the surface due to the external load and the small shape perturbation, and the other is caused by the surface energy. The first contribution tends to destabilize the surface since the stress near the surface valleys is slightly larger than the stress near the surface tips, which therefore produces a net atom flux from the valleys to the tips, while surface energy provides a stabilizing effect by reducing the perturbation and hence reducing the total surface energy. It has been shown that EM-induced atom current may damp this instability on a thin film surface [24]. However, in the configuration of modern IC interconnect where the metal surface is constrained by surrounding liners and soft low-k dielectrics (Fig. 1), the consequences of this stress-induced ATG instability have not yet been fully understood. While there is no free surface involved in the interconnect configuration, the essential physics that are required to activate an ATG type instability are still present [23], namely, interfacial transport of atoms and nonuniform stress along the interconnect. In previous studies of stress-driven atom transport using traditional finite-element models of electromigration [18], the shape of the metal-dielectric interface is not typically coupled with the atom flux. A free-boundary approach, where the interface shape can change due to a nonzero atomic flux, is required to investigate this instability.

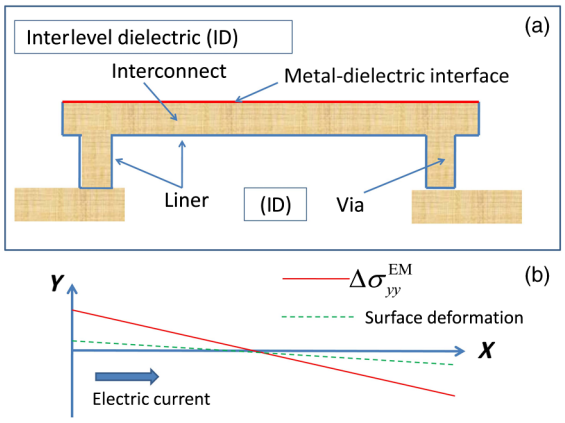

FIG. 1. Illustration of a typical interconnect. (a) Interfaces and different surrounding materials. (b) Stress and surface deformation caused by EM. The x axis is along the longitudinal direction of the interconnect, and the y axis is normal to the metal-dielectric interface.

II. INSTABILITY THEORY

It is instructive to confirm that the length scale introduced from the ATG theory is indeed comparable with the Blech length in a typical interconnect setup. The Blech length is determined by the balance of an EM-induced atom flux (pileup and depletion at the anode and cathode end, respectively) against a stress-driven atom flux due to the surrounding dielectric confinement. The ATG mechanism describes the stability of the interconnect-dielectric interface against an infinitesimal shape perturbation when the interconnect is subject to a significant longitudinal stress and atoms are allowed to move along the interface to minimize their chemical potential. When the interconnect length is longer than the Blech length, EM-induced transport cannot be completely shut off by the confinement stress from the dielectrics, and pileup and depletion occurring at the interconnect ends will develop over time and eventually lead to failure due to extrusion or void formation. On the other hand, when the interconnect length is longer than the ATG stability wavelength, small interface shape perturbation will be amplified over time due to the chemical potential difference of surface atoms at grooves and peaks under longitudinal thermal stress and may also lead to delamination failure or breakage if the shape perturbation becomes comparable to the interconnect thickness. A rough estimation of the length scales of these mechanisms can be obtained based on the two-dimensional (2D) picture shown in Fig. 1 using standard ATG theory without external confinement, a result that can be seen as

the limit of very weak confinement. For commonly used Cu interconnects, the Blech product is about 2000 A/cm. With a current density 2 MA/cm^2, this gives a Blech length $l_B \sim 10$ μm. Experimental measurements suggest that thermal stress in interconnects is on the order $\sigma_0 \sim 100$ MPa along the longitudinal direction of the interconnect at operational temperature. With the upper limit of copper-dielectric interface energy $\gamma \sim 1$ J/m^2 and Young's modulus $E \sim 100$ GPa, the estimated ATG instability length $l_c \sim E\gamma/\sigma_0^2$ is also $\sim$10 μm. It is known that the Blech length also depends on the level of thermal stress in the interconnect [8] according to

$$l_B = \frac{\Omega(\sigma_m - \sigma_t)}{Z^* e \rho j}, \tag{3}$$

where σ_t is a thermally induced hydrostatic stress. From this, a better comparison can be made between the stress-induced instability length scale l_c and the thermal stress-dependent Blech length in Eq. (3). This is shown in Fig. 2. Here, we relate the 2D hydrostatic stress to σ_o using $\sigma_t = (\sigma_0 + \sigma_{yy})/2$, where $\sigma_0 \sim 3\sigma_{yy}$ from typical experimental data.

Figure 2 shows that as the level of thermal stress increases, the critical length from the stress-driven surface instability decreases as $1/\sigma_t^2$ while the Blech length is a linear function. Given a large-enough σ_m and a relatively small current density, the two lengths predicted from these two mechanisms can cross each other at two points. Since failure is expected to occur at the shorter length, a switch from the Blech mechanism to the ATG mechanism is, thus, expected when the thermal stress level lies between the crossing points in Fig. 2. Another feature of this estimation is that the two mechanisms cross each other only at medium-to-low current density, implying that the Blech effect is always the leading cause of failure at large current density.

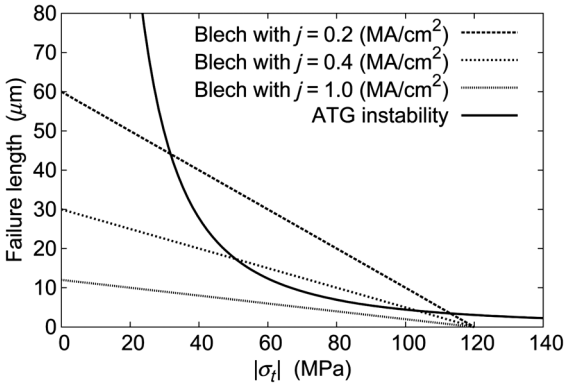

FIG. 2. Estimation of Cu interconnect failure length from ATG instability and Blech effect with difference current densities. Effective EM charge $Z^* = 5$, $\sigma_m = 120$ MPa.

The above analysis indicates that the maximum stress σ_m plays an important role in dictating the failure mechanism. Most previous works have focused on the void nucleation [8] mechanism since the stress required for void nucleation is smaller than that required for extrusion. Another mechanism that has been related to EM-induced failure is based on delamination between the metal and the dielectric layers [9]. The stress level required for the delamination is $\sigma_{\text{delam}} \sim (EG/h)^{1/2}$, where G is the interface adhesion energy, and h is the thickness of the metal conductor. In typical interconnects, the adhesion energy has the same magnitude as the interfacial energy γ, and the thickness h is usually much smaller than the length of the interconnect l. It is noteworthy that for typical values of these parameters, it is plausible that failure due to delamination requires a larger stress than failure due to stress-driven surface ATG instability. This is consistent with experiments, which have reported that an ATG-type surface instability can develop along the solid-state interface together with delamination [25].

We use Fig. 2 to demonstrate that the length scale introduced by an ATG-type surface instability failure mechanism in interconnects is comparable with the Blech length at experimentally relevant levels of thermal stress and electric current density. It uses the classic approach of calculating the back stress effect in the Blech condition in Eq. (2), first introduced by Korhonen *et al.* in the calculation of interconnect thermal stress [11]. This approach uses the strain due to the thermal expansion of the metal interconnect relative to the dielectric confinement of an interconnect to find the stress field within the conductor. From this, the effective modulus B can be calculated analytically using Eshelby's theory of elastic inhomogeneity [26]. Later finite-element studies of more realistic Cu interconnect geometries have shown that the effective elastic modulus for the expansion along the direction perpendicular to the metal-dielectric interface is also affected by the elastic property of both the liner material and the dielectric [27]. While such a confinement stress effect on interconnect failure has been discussed in previous theories, the context was limited to the void dynamical failure mechanism [28,29]. To our knowledge, previous classical theories of interconnect failure do not self-consistently incorporate the effect of confining materials on the ATG instability of the interconnect-dielectric interface. In this paper, we show that by incorporating the effect of confinement on a metal interconnect, the stress required to trigger an ATG-type surface instability can become comparable to the delamination stress, and hence a plausible mechanism for interconnect failure.

In the classical ATG mechanism, a traction-free boundary is used to calculate the stress field within the solid using a perturbation approach. However, the stress boundary condition for the shear component at the metal-dielectric interface is not clear, particularly in the presence of

EM-induced transport along the interface. To calculate the stress field within the interconnect, we employ a simplified stress boundary condition at the interface based on the same back stress argument in the Blech effect. As illustrated in Fig. 1(b), the effect of confinement generates an elastic back stress in response to the volumetric expansion from the EM-driven mass transport. If we characterize the local volume expansion in the interconnect by a deformation a from the non-EM state along the y direction (as the result of EM or TSM), the back stress confinement effect from the surrounding dielectrics can be written as $\sigma_{yy} = -ka$, where k is a force coefficient related to the elastic modulus of the confining materials. For the longest wavelength mode, which is usually associated with a surface instability, the deformation can be then written as $a = \epsilon \cos \omega x$ with $\omega = \pi/l$, amplitude ϵ, and the length of the interconnect l. Using this boundary condition, we solve the stress field within the interconnect. Following the classic perturbation approach [22], the stress components at the interface are

$$\sigma_{xx} = \sigma_0(1 + 2\epsilon\omega \cos \omega x), \tag{4}$$

$$\sigma_{yy} = -k\epsilon \cos \omega x, \tag{5}$$

$$\sigma_{xy} = \sigma_0 \epsilon\omega \sin \omega x. \tag{6}$$

Since the deformation amplitude ϵ is small, the change of the elastic energy density in the perturbed state relative to the uniform state can be expanded as a series in ϵ. To the first order in ϵ, it is

$$\Delta f_{\mathrm{el}} = -\left[\frac{2\epsilon\omega}{E}(1-\nu^2)\sigma_0^2 - \frac{k\epsilon}{E}\nu(1+\nu)\sigma_0\right]\cos \omega x, \tag{7}$$

where E is the Young's modulus, ν is the Poisson's ratio. The first term in Eq. (7) is the standard ATG expression. The second term accounts for the confinement effect of the dielectrics. Intuitively, the confinement should damp any shape change of the interconnect which is manifested as the minus sign in front of the second term.

The interface energy has a stabilizing effect in the ATG mechanism since any perturbation to the interface shape will increase the total surface energy (assuming an isotropic interface). It is straightforward to show that the change of the metal-dielectric interface energy density with a sinusoidal shape perturbation $\epsilon \cos \omega x$ is

$$\Delta f_s = \gamma\epsilon\omega^2 \cos \omega x, \tag{8}$$

where γ is the interfacial energy. For an interconnect below the Blech length where the EM-driven atom migration is completely balanced by the back stress effect, atoms in the interconnect may still move along the interface such as to minimize the total energy introduced from the shape perturbation $\Delta F = \int (\Delta f_{\mathrm{el}} + \Delta f_s)dx$. It can be shown that the additional stabilizing effect from the dielectric confinement predicts that the failure length of the classic ATG instability in Fig. 2 should be increased. This is found by applying the variational principle to ΔF with respect to the perturbation, which leads to the additional flux condition

$$-k\nu(1+\nu)\sigma_0 l^2 + 4\pi(1-\nu^2)\sigma_0^2 l - 4\pi^2\gamma E = 0. \tag{9}$$

Equation (9) expresses the balance of stress-driven transport and the stabilizing effects of interface energy and confinement. To further demonstrate the effect of confinement, a comparison of the critical interconnect failure length predicted by Eq. (9) with and without the confinement is shown in Fig. 3.

Equation (9) has two solution branches: one decreases as the stress level increases (dashed curve) and the other increases (dotted curve). At a given stress level, only the shorter length (dashed curve) is physically relevant since the instability would be active for any longer length. The turning point stress level $\sigma_{cc} \sim (Ek\gamma)^{1/3}$ (vertical dashed line in Fig. 3) corresponds to the stress below which the instability length diverges. Therefore, for any stress smaller than σ_{cc}, the instability mechanism cannot break interconnect of any length. This change of behavior is rather expected intuitively since the confinement stress can be seen as a stabilizing factor against surface instability. As we will see in what follows, σ_{cc} may lie within the relevant interconnect thermal stress levels if the confinement material is elastically very soft compared with the metal conductor. It is noted that in the theory above, we ignore the thermal stress component along the y direction since it is

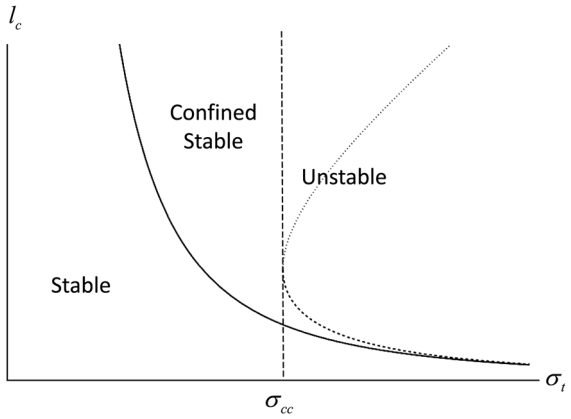

FIG. 3. Illustration of the critical interconnect failure length predicted by the standard ATG stability criterion (solid line) and the ATG stability criterion with confinement predicted by Eq. (9) (dashed and dotted curves). The vertical dashed line at the confined critical stress σ_{cc} gives the stability threshold predicted by the turning point of Eq. (9). Below σ_{cc}, all interconnect lengths are stable due to confinement. Above σ_{cc}, lengths longer than the lower (dashed) curve become unstable even if confined.

typically small compared with the other two normal components, particularly for low-k dielectric materials [12].

III. NUMERICAL VALIDATION

To validate our analytical prediction for the confinement effect in Fig. 3 [based on Eq. (9)], we also carry out phase-field (PF) simulations of the phenomenon described above. The PF method is a very useful approach for studying complex moving boundary problems such as dendritic solidification, grain growth in polycrystal, and second-phase precipitation [30–33]. By treating interfaces, diffusion, and elasticity in a single framework the PF model naturally couples mass transport to stress-driven interface motion. It has been used to model slit formation in EM [34,35], while in the context of stress-driven surface instability, the PF method has been shown to successfully capture the physics of the ATG instability of single-layer [36,37] and multilayer materials [38–40]. A recently developed atomic-level phase-field-crystal model has also been used to examine EM-induced void nucleation in metal interconnects [41].

The formulation of our PF method is based on an energy functional

$$F_{\mathrm{PF}} = \int [K|\nabla\phi|^2 + Hf_p(\phi) + f_{\mathrm{el}}(\phi,\vec{u})]dv, \qquad (10)$$

where ϕ is an order parameter, $\vec{u} = (u_x, u_y)$ is the displacement field, and K and H are constants. We define $\phi = 1$ as the metal interconnect and $\phi = 0$ as the confinement dielectric material. The first two terms in Eq. (10) produce an interface between $\phi = 0$ and $\phi = 1$ states with interfacial energy $\gamma = WH\int[|\partial\phi/\partial x|^2 + f_p(\phi)]dx$, where interface width $W = \sqrt{K/H}$, and x is the coordinate normal to the interface. The term $f_{\mathrm{el}}(\phi,\vec{u})$ is the elastic energy density, which is coupled with the PF parameter. Since our primary concern is the stress-driven transport of metal atoms, the elastic energy is coupled to ϕ such that f_{el} reduces to the standard expression of isotropic elastic energy $\frac{1}{2}\lambda(\epsilon_{ii})^2 + \mu\epsilon_{ij}^2$ (with strain ϵ_{ij} and elastic constants λ and μ) in the metal and to zero in the confinement dielectrics. Similarly to our previous analysis, in this approach the effect of confinement naturally leads to a stress boundary at the metal-dielectric interface where the normal stress component is proportional to the deformation of the interface from its equilibrium state. Evolution of the interface is captured by the motion of ϕ, which follows the conserved model B-type dynamics [42], given by

$$\frac{\partial\phi}{\partial t} = \nabla\cdot\left(M\nabla\frac{\delta F_{\mathrm{PF}}}{\delta\phi}\right), \qquad (11)$$

where M is the atomic mobility. Since the elastic process relaxed much faster compared to the interface motion, the displacement field is solved according to the elastostatic condition $\nabla\cdot\sigma = 0$, where $\sigma_{ij} = \delta F_{\mathrm{PF}}/\delta\epsilon_{ij}$. Since the metal-dielectric interface is the major transport path of atoms, Eq. (11) is modified slightly based on Ref. [37] to model interface diffusion. Since the traditional approach with a scalar mobility M that vanishes far away from the interface is shown to be inconsistent with the sharp interface theory asymptotically, we use the globally conserved tensorial (GCT) mobility method [37]. By replacing the scalar mobility in the classic PF method with a mobility tensor, materials transport is active only along the surface tangential direction in the diffused interface region. This GCT method is shown to convergence to the correct surface-diffusion dynamics in the sharp interface limit.

Numerical simulations are carried out in a two-dimensional rectangular grid using the semi-implicit Fourier method with $dx = 0.6$, $dt = 0.4$, and $M = 1.0$. Other parameters associated with the GCT method are taken from Ref. [37]. The simulation box size N_x changes from 200 to 400 based on a different interconnect length and $N_y = 512$. The metal interconnect is set to occupy the center region ($128 \le N_y < 384$) of the simulation box initially with a small sinusoidal shape perturbation. The periodic boundary condition is applied.

Shape deformation of a confined interconnect from our PF simulations is demonstrated in Fig. 4(a). An initial small shape perturbation is amplified over time. Interconnect stability can then be determined by monitoring the change of the total surface energy from an initial small-amplitude sinusoidal shape perturbation. The instability length extracted from the PF results is compared with the prediction of Eq. (9) for $\sigma_0 > \sigma_{cc}$ in Fig. 4(b) with two different confinement force coefficients k. To demonstrate its difference from the standard ATG theory, the instability length is scaled by the standard ATG instability length l_c^0 in the plot. Horizontal stress is scaled by $\sigma_{\mathrm{PF}} = \gamma/W$. Since the thermal stress component along the y direction is typically small compared with others (especially for low-k dielectric materials) [12], we take the same approximation as we did in deriving the theory [Eq. (9)] where the thermal stress along the y direction has been ignored.

Figure 4(b) shows that by including the external confinement stress from surrounding materials, the critical surface instability length can be significantly modified. The instability can be active only above the critical stress σ_{cc} in the tensile regime as expected from our analysis shown in Fig. 3. The critical stress σ_{cc} depends on the confinement strength. For weak confinement, σ_{cc} becomes small as one would expect and $\sigma_{cc} \to 0$ with vanishing confinement (i.e., the instability relation becomes the standard ATG relation). In the context of the relation between the critical interconnect length and the thermal stress demonstrated in Fig. 2, a length-independent thermal stress level σ_{cc} must be reached first before the surface instability mechanism becomes relevant. At a given σ_0, the instability may or may

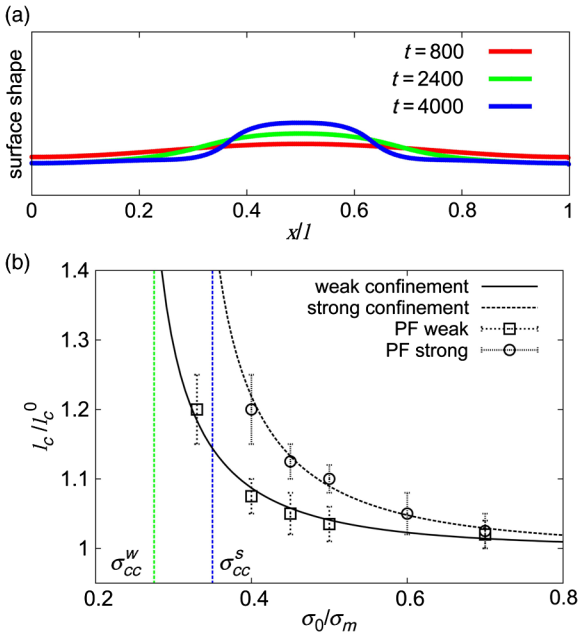

FIG. 4. (a) Destabilization of interconnect shape under weak confinement. (b) Failure length of interconnect under confinement as a result of a different horizontal stress. Data points are PF simulations and curves are analytical predictions (see text). The error bars in the PF data are computed as the variation between two independent simulation samples. σ_{cc} for strong and weak cases is marked by the vertical dashed lines. Confinement force parameter $kh/E = 0.01$ for weak confinement and $kh/E = 0.02$ for strong confinement. See text for other parameters.

not manifest itself, depending on the confinement strength since σ_{cc} depends on the confinement materials and the critical interconnect length diverges for $\sigma_0 \leq \sigma_{cc}$.

To estimate the order of this critical stress σ_{cc} we need to relate the confinement force coefficient k to the properties of the surrounding dielectric materials. Since we assume the confinement stress is generated elastically by the surrounding materials in response to the interconnect deformation, one can simply write $k \sim E_c/h_c$, where E_c is the elastic modulus of the confinement and h_c is an effective thickness of the confinement materials. E_c is similar to the effective elastic modulus B when calculated based on the expansion normal to the metal-dielectric interface. For soft low-k dielectric materials with thin liner and low conductor thickness-to-width ratio, it can be brought down to the order of a few gigapascals [27]. The thickness of confinement material usually satisfies $h_c/h \gg 1$ since it is a common assumption used in the effective modulus theory that the size of the confinement materials is much larger than the thickness of the interconnect. With the thickness of the interconnect $h \sim 0.1$ μm, $h_c/h \sim 10$–100, copper-elastic modulus $E \sim 100$ GPa, effective modulus $B \sim 5$ GPa for soft low-k dielectrics, surface-adhesion energy $\gamma \sim 0.1$ J/m^2, the length-independent critical stress level σ_{cc} is estimated $\sim$100 MPa, which is on the same order of the delamination stress σ_{delam}. Since σ_{cc} is estimated to be within the relevant thermal stress level for a soft low-k confinement dielectric, our results show that it is plausible that the Blech-to-ATG switching mechanism discussed in relation to Fig. 2 could occur for a confined metal interconnect in the presence of electric-current density.

IV. DISCUSSIONS AND CONCLUSIONS

In this work, we examine failure in metal interconnects via the classic ATG mechanism of thermal stress-driven surface instability modified for dielectric confinement. The confinement of the interconnect by a surrounding dielectric changes the stress-driven instability wavelength predicted by the classic ATG mechanism qualitatively, with a critical stress σ_{cc} being required in the tensile regime to trigger the instability regardless of the wavelength. In the case of soft low-k dielectric confinement, this instability may be triggered with thermal stress on the order of a few hundred megapascals, which corresponds to a σ_{cc} smaller than the maximum stress σ_m required in the Blech condition. Our results thus predict that for commonly observed thermal stresses acting in commercial metal interconnects, the critical failure length from a thermal stress-driven surface instability is comparable with the Blech length under typical EM electric-current density. Moreover, for certain ranges of thermal stress, the stress-driven instability investigated here may be the main mechanism responsible for the failure of the interconnect since the critical instability length predicted by the confined ATG mechanism could become shorter than the Blech length. Although the stress boundary condition at the interconnect-dielectric interface is not exact, its validity is partially supported by previous works on the Blech effect, and shows consistency with experiments. Despite the simplifications we made in our analytical derivations, the predicted instability mechanism proposed in this work appears to be an additional relevant factor to be considered in the design and manufacture of metal interconnects, especially for those under weak confinement.

ACKNOWLEDGMENTS

We thank The National Science and Engineering Research Council of Canada and the Canada Research Chairs (CRC) program for funding, and Compute Canada for computing resources.

[1] K. N. Tu, Recent advances on electromigration in very-large-scale-integration of interconnects, J. Appl. Phys. **94**, 5451 (2003).

[2] R. L. de Orio, H. Ceric, and S. Selberherr, Physically based models of electromigration: From Blacks equation to modern TCAD models, Microelectron. Reliab. **50**, 775 (2010).

[3] H. Ceric and S. Selberherr, Electromigration in submicron interconnect features of integrated circuits, Mater. Sci. Eng. R **71**, 53 (2011).

[4] I. A. Blech, Electromigration in thin aluminum films on titanium nitride, J. Appl. Phys. **47**, 1203 (1976).

[5] Ennis T. Ogawa, Alexander J. Bierwag, Ki-Don Lee, Hideki Matsuhashi, Patrick R. Justison *et al.*, Direct observation of a critical length effect in dual-damascene Cu/oxide interconnects, Appl. Phys. Lett. **78**, 2652 (2001).

[6] Seung-Hyun Rhee, Yong Du, and Paul S. Ho, Thermal stress characteristics of Cu/oxide and Cu/low-*k* submicron interconnect structures, J. Appl. Phys. **93**, 3926 (2003).

[7] Paul S. Ho, Ki-Don Lee, Sean Yoon, Xia Lu, and Ennis T. Ogawa, Effect of low *k* dielectrics on electromigration reliability for Cu interconnects, Mater. Sci. Semicond. Process. **7**, 157 (2004).

[8] J. R. Lloyd, Electromigration and mechanical stress, Microelectron. Eng. **49**, 51 (1999).

[9] J. R. Lloyd, C. E. Murray, T. M. Shaw, M. W. Lane, X.-H. Liu, and E. G. Liniger, Theory for electromigration failure in Cu conductors, AIP Conf. Proc. **23**, 817 (2006).

[10] Frank. L. Wei, Chee Lip Gan, Tam Lyn Tan, Christine S. Hau-Riege, Amit P. Marathe, Joost J. Vlassak, and Carl V. Thompson, Electromigration-induced extrusion failures in Cu/low-*k* interconnects, J. Appl. Phys. **104**, 023529 (2008).

[11] M. A. Korhonen, R. D. Black, and Che-Yu Li, Stress relaxation of passivated aluminum line metallizations on silicon substrates, J. Appl. Phys. **69**, 1748 (1991).

[12] M. A. Korhonen, P. Borgesen, K. N. Tu, and Che-Yu Li, Stress evolution due to electromigration in confined metal lines, J. Appl. Phys. **73**, 3790 (1993).

[13] J. J. Clement and C. V. Thompson, Modeling electromigration-induced stress evolution in confined metal lines, J. Appl. Phys. **78**, 900 (1995).

[14] P.-C. Wang, G. S. Cargill III, I. C. Noyan, and C.-K. Hu, Electromigration-induced stress in aluminum conductor lines measured by x-ray microdiffraction, Appl. Phys. Lett. **72**, 1296 (1998).

[15] M. E. Sarychev, Yu. V. Zhitnikov, L. Borucki, C.-L. Liu, and T. M. Makhviladze, General model for mechanical stress evolution during electromigration, J. Appl. Phys. **86**, 3068 (1999).

[16] A. Wikstrm, P. Gudmundson, and S. Suresh, Analysis of average thermal stresses in passivated metal interconnects, J. Appl. Phys. **86**, 6088 (1999).

[17] Jie-Hua Zhao, Wen-Jie Qi, and Paul S. Ho, Thermomechanical property of diffusion barrier layer and its effect on the stress characteristics of copper submicron interconnect structures, Microelectron. Reliab. **42**, 27 (2002).

[18] N. Singh, A. F. Bower, and S. Shankar, A three-dimensional model of electromigration and stress induced void nucleation in interconnect structures, Model. Simul. Mater. Sci. Eng. **18**, 065006 (2010).

[19] A. Tezaki, T. Mineta, H. Egawa, and T. Noguchi, Measurement of three dimensional stress and modeling of stress-induced migration failure in aluminium interconnects, Proc. Reliab. Phys. Symp. **28**, 221 (1990).

[20] Christine S. Hau-Riege, Stefan P. Hau-Riege, and Amit P. Marathe, The effect of interlevel dielectric on the critical tensile stress to void nucleation for the reliability of Cu interconnects, J. Appl. Phys. **96**, 5792 (2004).

[21] L. Angheluta and J. Mathiesen, Thermodynamics of stressed solids: Slow deformation and roughening of material interfaces, Eur. Phys. J. Spec. Top. **178**, 123 (2009).

[22] R. J. Asaro and W. A. Tiller, Interface morphology development during stress corrosion cracking, Metall. Trans. **3**, 1789 (1972).

[23] M. Grinfeld, The stress driven instability in elastic crystals: Mathematical models and physical manifestations, J. Nonlinear Sci. **3**, 35 (1993).

[24] V. Tomar, M. R. Gungor, and D. Maroudas, Current-Induced Stabilization of Surface Morphology in Stressed Solids, Phys. Rev. Lett. **100**, 036106 (2008).

[25] Soonwoo Chah, Jaan Noolandi, and Richard N. Zare, Undulatory delamination of thin polymer films on gold surfaces, J. Phys. Chem. **109**, 19416 (2005).

[26] J. D. Eshelby, The determination of the elastic field of an ellipsoidal inclusion, and elated problems, Proc. R. Soc. A **241**, 376 (1957).

[27] J. J. Clement and C. V. Thompson, The effects of the mechanical properties of the confinement material on electromigration in metallic interconnects, J. Mater. Res. **15**, 1797 (2000).

[28] M. R. Gungor and D. Maroudas, Modeling of electromechanically-induced failure of passivated metallic thin films used in device interconnections, Int. J. Fract. **109**, 47 (2001).

[29] D. Maroudas, Surface morphological response of crystalline solids to mechanical stresses and electric fields, Surf. Sci. Rep. **66**, 299 (2011).

[30] Nikolas Provatas, Nigel Goldenfeld, and Jonathan Dantzig, Efficient Computation of Dendritic Microstructures Using Adaptive Mesh Refinement, Phys. Rev. Lett. **80**, 3308 (1998).

[31] Alain Karma, Phase-Field Formulation for Quantitative Modeling of Alloy Solidification, Phys. Rev. Lett. **87**, 115701 (2001).

[32] V. Vaithyanathan, C. Wolverton, and L. Q. Chen, Multiscale Modeling of Precipitate Microstructure Evolution, Phys. Rev. Lett. **88**, 125503 (2002).

[33] Nikolas Provatas and Ken Elder, *Phase-Field Methods in Material Science and Engineering* (Wiley, Weinheim, 2010).

[34] M. Mahadevan and R. M. Bradley, Simulations and theory of electromigration-induced slit formation in unpassivated single-crystal metal lines, Phys. Rev. B **59**, 11037 (1999).

[35] D. N. Bhate, A. Kummar, and A. F. Bower, Diffuse interface model for electromigration and stress voiding, J. Appl. Phys. **87**, 1712 (2000).

[36] Judith Müller and Martin Grant, Model of Surface Instabilities Induced by Stress, Phys. Rev. Lett. **82**, 1736 (1999).

[37] C. Gugenberger, R. Spatschek, and K. Kassner, Comparison of phase-field models for surface diffusion, Phys. Rev. E **78**, 016703 (2008).

[38] N. Sridhar, J. M. Rickman, and D. J. Srolovitz, Multilayer film stability, J. Appl. Phys. **82**, 4852 (1997).

[39] N. Sridhar, J. M. Rickman, and D. J. Srolovitz, Microstructural stability of stressed lamellar and fiber composites, Acta Mater. **45**, 2715 (1997).

[40] B. G. Chirranjeevi, T. A. Abinandanan, and M. P. Gururajan, A phase field study of morphological instabilities in multilayer thin films, Acta Mater. **57**, 1060 (2009).

[41] Nan Wang, Kirk H. Bevan, and Nikolas Provatas, Phase-Field-Crystal Model for Electromigration in Metal Interconnects, Phys. Rev. Lett. **117**, 155901 (2016).

[42] P. C. Hohenberg and B. I. Halperin, Theory of dynamical critical phenomemon, Rev. Mod. Phys. **49**, 435 (1977).